Available online at www.sciencedirect.com
SCIENCE DIRECT®
ELSEVIER
International Journal of Solids and Structures 41 (2004) 7111–7128
INTERNATIONAL JOURNAL OF SOLIDS and STRUCTURES
www.elsevier.com/locate/ijsolstr

A novel hybrid finite element with a hole for analysis of plane piezoelectric medium with defects

Xinwei Wang *, Yong Zhou, Wanlin Zhou

The Aeronautical Science Key Lab for Smart Materials and Structures, Nanjing University of Aeronautics and Astronautics, Nanjing 210016, PR China

Received 13 September 2003; received in revised form 8 June 2004
Available online 20 July 2004

Abstract

A method is presented to formulate a novel hybrid finite element to obtain accurate distributions of mechanical and electrical quantities around a hole in plane piezoelectric mediums. The complex variable method is used in conjunction with Reissner's variational principle to formulate a hybrid special element with an elliptical hole. Detailed derivations are given and numerical examples are performed to demonstrate the accuracy and efficiency of the novel special element. Accurate results around the hole boundary are obtained for infinite and finite piezoelectric medium by using proposed special element.

Keywords: Hybrid finite element; Piezoelectric; Complex variable; Hole

1. Introduction

PZT materials are widely used as sensors/actuators in smart structures due to their fast response and low energy consumption. There are a lot of articles dealing with the damages (cracks) as well as inclusions of PZT material itself by using analytical approaches (See, for example, a review paper by Chen and Yu, 1999; papers by Sosa, 1991, 1992; Chung and Ting, 1996; Lu and Williams, 1998; Deng and Wang, 2002). As is well known that analytical solutions can be obtained only for the simple cases, therefore, numerical methods, such as the finite element method, boundary element method, and/or the coupled FEM–BEM, should be resorted for obtaining solutions in general complicated cases. Details on the modeling of piezoelectric materials and smart structures by conventional finite elements and boundary element method may be referred, for example, papers by Benjeddou (2000), Lu and Maharenholtz (1994), and Denda and Lua (1999).

* Corresponding author. Tel.: +86-2584-893466; fax: +86-2584-891488.
E-mail address: wangx@nuaa.edu.cn (X. Wang).

0020-7683/$ - see front matter © 2004 Elsevier Ltd. All rights reserved.
doi:10.1016/j.ijsolstr.2004.06.012

It is also well known, however, that it is costly to model a crack or hole by using ordinary finite elements. Special elements employing hybrid formulations have been succeeded for analyzing crack problems in plane elasticity (Tong et al., 1977; Zienkiewicz and Taylor, 2000), laminated plates with an elliptical hole (Chen, 1994; Zhan et al., 2003), and problems of cracks at bimaterial interfaces (Lee and Gao, 1995; Sze and Wang, 2000; Chen et al., 2001). It is demonstrated that hybrid finite elements have the advantages of high accuracy for hole and crack problems. Recently, the finite element method for ordinary materials (Sze and Wang, 2000) has been extended to piezoelectric materials for computing edge singularities (Sze et al., 2001).

In this paper, a special hybrid finite element with an elliptical hole is developed herein based on the Reissner's variational principle by EerNisse (1983). Complex variable method is used to obtain the approximate solutions of the stresses, displacements, and electric displacements within the element domain. In other words, the assumed stresses, displacements, and electric displacements for the special hybrid element satisfy the governing differential equations and compatibility equations in advance. In this way, highly efficient novel special elements can be formulated to model the piezoelectric medium with a hole or crack. It should be mentioned the more general variational principle of piezoelectricity with six kinds of independent variables given by Lu and Maharenholtz (1994) could be used for developing various special finite or boundary elements.

Numerical examples with known analytical solutions by Sosa (1991) are performed to demonstrate the accuracy and efficiency of the novel special elements. Accurate results around the hole boundary are obtained for infinite and finite piezoelectric mediums by using only one special element. The behaviors of finite plates with an elliptical hole with semi-axes of a and b under combined mechanical and electrical loadings are then studied. It is found that the relationship between the logarithm concentration factors of tangential stress, electrical displacement, and electrical field at notch tip and logarithm b/a ratio is fairly linear under certain loading cases.

2. Basic formulations

Using the complex variable formulation as described by Sosa (1991), the stress functions $U(x,y)$, and the induction function $\Psi(x,y)$ for piezoelectric media with defects in two dimensions can be expressed by using the following two complex functions, namely,

$$U(x,y) = 2\mathrm{Re}\sum_{k=1}^{3} U_k(z_k), \quad \Psi(x,y) = 2\mathrm{Re}\sum_{k=1}^{3} \lambda_k \frac{dU_k(z_k)}{dz_k} \tag{1a,b}$$

where the symbol Re represents the real part of a complex function, λ_k and the complex variable z_k are defined as

$$z_k = x + \mu_k y \tag{2a}$$

$$\lambda_k(\mu_k) = -\frac{b(\mu_k)}{\delta(\mu k)} = -\frac{(b_{21}+b_{13})\mu_k^2 + b_{22}}{\delta_{11}\mu_k^2 + \delta_{22}}, \quad \delta(\mu_k) \neq 0 \tag{2b}$$

The complex variable μ_k ($k = 1, 2, 3$) is the roots of the following equation:

$$a_{11}\delta_{11}\mu^6 + (a_{11}\delta_{22} + 2a_{12}\delta_{11} + a_{33}\delta_{11} + b_{21}^2 + b_{13}^2 + 2b_{21}b_{13})\mu^4 + (a_{22}\delta_{11} + 2a_{12}\delta_{22} + a_{33}\delta_{22} + 2b_{21}b_{22} + 2b_{22}b_{13})\mu^2 + (a_{22}\delta_{22} + b_{22}^2) = 0 \tag{3}$$

For transversely isotropic (x_1x_2 plane) piezoelectric materials with poling direction in the x_3 direction and for plane strain condition ($\varepsilon_{22} = \varepsilon_{32} = \varepsilon_{12} = E_2 = 0$), the remaining notations appeared in Eqs. (2b) and (3) can be found in the work of Sosa (1991).

Consider the case of plane strain. Now let the y be the poling direction and introduce the following notations, Φ_k, Φ'_k $(k = 1, 2, 3)$, namely,

$$\Phi_k(Z_k) = U'_k = \frac{dU_k}{dz_k}, \quad \Phi'_k = \frac{d\Phi_k}{dz_k} \tag{4a,b}$$

The stress field, displacement field and electrical field can be obtained once the functions in Eq. (4a,b) are known.

Consider a piezoelectric plate containing an elliptical hole with semi-axes of a and b. To apply the hole-boundary conditions conveniently, conformal transformations proposed by Lekhnitskii (1981), Eq. (5), are performed to map the exterior of three ellipses contained in the Z_j plane onto the exterior of the unit circle located in the ξ_j planes,

$$Z_j = \frac{a - \mathrm{i}\mu_j b}{2}\xi_j + \frac{a + \mathrm{i}\mu_j b}{2}\xi_j^{-1} \quad (j = 1, 2, 3) \tag{5}$$

The inverse mapping ξ_j is given by

$$\xi_j = \frac{Z_j \pm \sqrt{Z_j^2 - (a - \mathrm{i}\mu_j b)(a + \mathrm{i}\mu_j b)}}{a - \mathrm{i}\mu_j b} \quad (j = 1, 2, 3) \tag{6}$$

In terms of the variable ξ_k, the stress field, displacement field and electrical field can be written as

$$\sigma_{xx} = 2\mathrm{Re}\sum_{k=1}^{3}\mu_k^2\phi'_k(\xi_k)/Z'_k(\xi_k); \quad \sigma_{yy} = 2\mathrm{Re}\sum_{k=1}^{3}\phi'_k(\xi_k)Z'_k(\xi_k);$$

$$\sigma_{xy} = -2\mathrm{Re}\sum_{k=1}^{3}\mu_k\phi'_k(\xi_k)/Z'_k(\xi_k); \quad u = 2\mathrm{Re}\sum_{k=1}^{3}p_k\phi_k(\xi_k) + \omega_0 y + u_0;$$

$$v = 2\mathrm{Re}\sum_{k=1}^{3}q_k\phi_k(\xi_k) - \omega_0 x + v_0 \tag{7a–e}$$

$$D_1 = 2\mathrm{Re}\sum_{k=1}^{3}\lambda_k\mu_k\phi'_k(\xi_k)/Z'_k(\xi_k); \quad D_2 = -2\mathrm{Re}\sum_{k=1}^{3}\lambda_k\phi'_k(\xi_k)/Z'_k(\xi_k) \tag{7f, g}$$

$$E_1 = 2\mathrm{Re}\sum_{k=1}^{3}(b_{13} + \delta_{11}\lambda_k)\mu_k\Phi'_k(\xi_k)/Z'(\xi_k)$$

$$E_2 = -2\mathrm{Re}\sum_{k=1}^{3}(b_{21}\mu_k^2 + b_{22} + \delta_{22}\lambda_k)\Phi'_k(\xi_k)/Z'(\xi_k) \tag{7h, i}$$

$$\varphi = -2\mathrm{Re}\sum_{k=1}^{3}(b_{13} + \delta_{11}\lambda_k)\mu_k\Phi_k(\xi_k) + \varphi_0 \tag{7j}$$

where

$$Z'_k(\xi_k) = \frac{dZ_k}{d\xi_k} = \frac{a - \mathrm{i}\mu_k b}{2} - \frac{a + \mathrm{i}\mu_k b}{2}\xi_k^{-2} \tag{8}$$

All other symbols appeared in Eq. (7) can be found in the work of Sosa (1991).

For the D–P condition (traction-free and charge-free) along the cavity boundary, one has

$$\mathrm{Re}\sum_{k=1}^{3}\phi_k(\xi_k)=0,\quad \mathrm{Re}\sum_{k=1}^{3}\mu_k\phi_k(\xi_k)=0,\quad \mathrm{Re}\sum_{k=1}^{3}\lambda_k\phi_k(xi_k)=0 \tag{9a–c}$$

or in matrix notation:

$$\begin{pmatrix}1 & 1 & 1\\ \bar{\mu}_1 & \bar{\mu}_2 & \bar{\mu}_3\\ \bar{\lambda}_1 & \bar{\lambda}_2 & \bar{\lambda}_3\end{pmatrix}\begin{Bmatrix}\bar{\phi}_1\\ \bar{\phi}_2\\ \bar{\phi}_3\end{Bmatrix}=-\begin{pmatrix}1 & 1 & 1\\ \mu_1 & \mu_2 & \mu_3\\ \lambda_1 & \lambda_2 & \lambda_3\end{pmatrix}\begin{Bmatrix}\phi_1\\ \phi_2\\ \phi_3\end{Bmatrix} \tag{10}$$

Eq. (10) can be written as

$$\begin{Bmatrix}\bar{\phi}_1\\ \bar{\phi}_2\\ \bar{\phi}_3\end{Bmatrix}=\begin{pmatrix}E_{11} & E_{12} & E_{13}\\ E_{21} & E_{22} & E_{23}\\ E_{31} & E_{32} & E_{33}\end{pmatrix}\begin{Bmatrix}\phi_1\\ \phi_2\\ \phi_3\end{Bmatrix} \tag{11}$$

Generally speaking, it is impossible to find a closed form solutions for $\phi_k(\xi_k)$ for arbitrary boundary conditions. A finite series formulation is commonly adopted, namely,

$$\phi_1(\xi_1)=\sum_{j=-N}^{M}A_j\xi_1^j,\quad \phi_2(\xi_2)=\sum_{j=-N}^{M}B_j\xi_2^j,\quad \phi_3(\xi_3)=\sum_{j=-N}^{M}C_j\xi_3^j \tag{12a–c}$$

where A_j, B_j, C_j are complex coefficients to be determined by the boundary conditions.

Without loss of the generality, set M equal N. Note that terms with $j=0$ in Eq. (12a–c) contribute no stresses and electric displacements and thus are discarded. After satisfying the boundary conditions, Eq. (9a–c), on the elliptical hole boundary and note the fact of that $\bar{\xi}_k^j=\xi_k^{-j}$ on the unit circle, the total number of independent coefficients is reduced to half. In other words, the total number of independent coefficients in Eq. (12) is now $6N$.

3. Reissner's variational principle

Following EerNisse (1983), Reissner's Variational Functional can be expressed as

$$\begin{aligned}\prod_R=\int_\Omega\left[u_{i,j}\sigma_{ij}-\frac{1}{2}s^D_{ijkl}\sigma_{ij}\sigma_{kl}-u_if_i+\varphi_{,i}D_i+\frac{1}{2}\beta^\sigma_{ij}D_iD_j+\varphi q_\mathrm{b}-g_{kij}\sigma_{ij}D_k\right]\mathrm{d}v+\int_{S_\mathrm{u}}(\tilde{u}_i\\ -u_i)\sigma_{ij}n_j\mathrm{d}s+\int_{S_\varphi}(\tilde{\varphi}-\varphi)D_jn_j\mathrm{d}s-\int_{S_\sigma}u_i\tilde{T}_i\mathrm{d}s+\int_{S_\omega}\varphi\tilde{q}_s\mathrm{d}s\end{aligned} \tag{13}$$

where s^D_{ijkl}, β^σ_{ij}, g_{kij} are the compliance tensor of the material measured at zero electric displacement, the dielectric impermeability tensor measured at zero stress, and the piezoelectric tensor; u_i, σ_{ij}, φ, D_i are the displacement vector, stress tensor, the electric potential, and electric displacement vector, f_i, q_b are the body force vector and the body charge vector, respectively. The quantities with symbol $\tilde{}$ represent the known quantity. And S_u, S_σ, S_φ, S_ω represents the boundary with given displacement, traction forces, electric potential, and the electric displacement, respectively.

The special element matrices are to be formulated from the element's functional $\prod_R^E$ by assuming u_i, σ_{ij}, φ, D_i in the element domain and $\tilde{u}_i$, $\tilde{\varphi}$ along the element outer boundary. Theoretically all these quantities can be assumed independently, however, they are to be chosen that the governing differential equations and compatibility equations be satisfied in advance. Thus, the functional defined in the element domain is simplified as

$$\prod_R^E = \int_{S_E} \tilde{u}_i \sigma_{ij} n_j \mathrm{d}s - \frac{1}{2}\int_{S_E} u_i \sigma_{ij} n_j \mathrm{d}s + \int_{S_E} \tilde{\varphi} D_j n_j \mathrm{d}s - \frac{1}{2}\int_{S_E} \varphi D_j n_j \mathrm{d}s - \int_{S_\sigma} u_i \widetilde{T}_i \mathrm{d}s + \int_{S_\omega} \varphi \tilde{q}_s \mathrm{d}s \tag{14}$$

Note that the components of body force vector and the body charge vector f_i, q_b are assumed zero in writing Eq. (14) and S_E is the element boundary. The last two integrals on the right-hand side of Eq. (14) should be dropped if the element is surrounded by special or conventional elements, the case considered in the following derivations. The quantities with symbol $\tilde{}$ represent the quantities only on the element outer boundary, since the D–P condition along the hole boundary has been satisfied in advance. It should be emphasized that only boundary integrals are involved in Eq. (14), different from the sub-region mixed functional (Zhao and Shan, 1991). Detail discussions may be referred to the book written by Zienkiewicz and Taylor (2000).

For convenience, introduce following notations:

$$\boldsymbol{\sigma} = \begin{Bmatrix} \sigma_{xx} \\ \sigma_{yy} \\ \sigma_{xy} \\ D_x \\ D_y \end{Bmatrix}, \quad \mathbf{u} = \begin{Bmatrix} u \\ v \\ \varphi \end{Bmatrix}, \quad \mathbf{t} = \begin{Bmatrix} t_x \\ t_y \\ q \end{Bmatrix}, \quad \boldsymbol{\beta} = \begin{Bmatrix} \beta_1 \\ \beta_2 \\ \cdot \\ \cdot \\ \beta_n \end{Bmatrix}, \quad \boldsymbol{\delta} = \begin{Bmatrix} u_1 \\ v_1 \\ \varphi_1 \\ \cdot \\ u_m \\ v_m \\ \varphi_m \end{Bmatrix} \tag{15a–e}$$

where n is the number of unknowns, and m is the number of nodal points of the special element. Assuming u_i, σ_{ij}, φ, D_i in the element domain yields

$$\boldsymbol{\sigma} = \mathbf{S}\boldsymbol{\beta}, \quad \mathbf{u} = \mathbf{U}\boldsymbol{\beta} \tag{16a,b}$$

where elements containing in matrices $\mathbf{S}$ and $\mathbf{U}$ are interpolation functions to be defined in Section 4. Then, one can evaluate $\mathbf{t}$ at the element boundary, namely,

$$\mathbf{t} = \mathbf{N}\boldsymbol{\sigma} = \mathbf{N}\mathbf{S}\boldsymbol{\beta} \tag{17}$$

Let n_x, n_y be the components of the unit normal to the element external boundary, thus matrix N in Eq. (17) can be expressed as

$$\mathbf{N} = \begin{bmatrix} n_x & 0 & n_y & 0 & 0 \\ 0 & n_y & n_x & 0 & 0 \\ 0 & 0 & 0 & n_x & n_y \end{bmatrix} \tag{18}$$

The external boundary displacement vector and electric potential, $\tilde{\mathbf{u}}$, is independently assumed in terms of the nodal displacements and electric potentials, namely,

$$\tilde{\mathbf{u}} = \mathbf{L}\boldsymbol{\delta} \tag{19}$$

where elements of matrix L are the interpolation functions defined only along the element external boundary. To be jointed with special or conventional elements, the interpolation functions for the special element developed herein are chosen to be displacement shape functions of the adjacent conventional elements.

Neglect the body forces, body charges, and the boundary loadings, the functional for the special element can be symbolically written as

$$\prod_R^E = \boldsymbol{\beta}^{\mathrm{T}}\left(\int_{S_e} (\mathbf{N}\mathbf{S})^{\mathrm{T}}\mathbf{L}\mathrm{d}s)\right)\boldsymbol{\delta} - \frac{1}{2}\boldsymbol{\beta}^{\mathrm{T}}\left(\int_{S_e} (\mathbf{N}\mathbf{S})^{\mathrm{T}}\mathbf{U}\mathrm{d}s\right)\boldsymbol{\beta} = \boldsymbol{\beta}^{\mathrm{T}}\mathbf{G}\boldsymbol{\delta} - \frac{1}{2}\boldsymbol{\beta}^{\mathrm{T}}\mathbf{H}\boldsymbol{\beta} \tag{20}$$

where

$$\mathbf{G} = \int_{S_e} (\mathbf{NS})^{\mathrm{T}} \mathbf{L} \mathrm{d}s, \quad \mathbf{H} = \frac{1}{2} \int_{S_e} [(\mathbf{NS})^{\mathrm{T}} \mathbf{U} + \mathbf{U}^{\mathrm{T}} (\mathbf{NS})] \mathrm{d}s \tag{21a,b}$$

Since $\boldsymbol{\beta}$ and $\boldsymbol{\delta}$ are assumed independently, set $\partial \prod_R^E / \partial \boldsymbol{\beta} = 0$ yields

$$\mathbf{G}\boldsymbol{\delta} - \mathbf{H}\boldsymbol{\beta} = \mathbf{0} \tag{22}$$

or

$$\boldsymbol{\beta} = \mathbf{H}^{-1}\mathbf{G}\boldsymbol{\delta} \tag{23}$$

Substituting Eq. (23) into Eq. (20)

$$\prod_R^E = \frac{1}{2} \boldsymbol{\delta}^{\mathrm{T}} \mathbf{G}^{\mathrm{T}} \mathbf{H}^{-1} \mathbf{G} \boldsymbol{\delta} = \frac{1}{2} \boldsymbol{\delta}^{\mathrm{T}} \mathbf{K} \boldsymbol{\delta} \tag{24}$$

$$\mathbf{K}\boldsymbol{\delta} = \partial \prod_R^E / \partial \boldsymbol{\delta} = (\mathbf{G}^{\mathrm{T}} \mathbf{H}^{-1} \mathbf{G}) \boldsymbol{\delta} \tag{25}$$

Thus, the stiffness matrix for the special element is obtained. The $\mathbf{K}$ in Eq. (25) could be viewed as a "standard stiffness matrix" (Zienkiewicz and Taylor, 2000). As was demonstrated by Chen (1994), the special element developed in this way could be conveniently used to join other variationally compatible elements in the stress analyses of laminated plates, such as the conventional finite elements or the special elements themselves.

4. Eight-node special hybrid finite element

As an example, an eight-node special hybrid finite element, schematically shown in Fig. 1, is considered. Elements with different nodes (e.g. 4, 16, or more nodes) could be formulated in a similar way without any difficulty (Lee and Gao, 1995). An elliptical hole is located at the element center. Each node has three degrees of freedom (DOFs). For example, at node 1, the three DOFs are u_1, v_1, φ_1. The poling direction is assumed in the y-direction. The lengths of the semi-axes of the hole are a and b. The side lengths of the element are denoted by L_{13}, L_{35}, L_{57}, L_{71}, respectively.

For developing the special element, Eqs. (11) and (12) are used to determine the stress and electric displacement within the element, namely, to obtain Eq. (16a). Set $N = 4$, then $\boldsymbol{\beta}$ is

$$\boldsymbol{\beta}^{\mathrm{T}} = \{A_{x1}, A_{y1}, \ldots, A_{x4}, A_{y4}, B_{x1}, B_{y1}, \ldots, B_{x4}, B_{y4}, C_{x1}, C_{y1}, \ldots, C_{x4}, C_{y4}\} \tag{26}$$

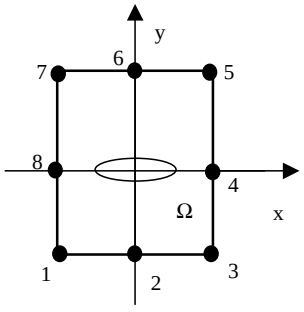

Fig. 1. An eight-node element with a center elliptical hole.

where elements of vector $\boldsymbol{\beta}$ are parts of the complex coefficients in Eq. (12) and defined by

$$A_k = A_{xk} + \mathrm{i}A_{yk}, \quad B_k = B_{xk} + \mathrm{i}B_{yk}, \quad C_k = C_{xk} + \mathrm{i}C_{yk} \quad (k = 1, 2, 3, 4, \ \mathrm{i} = \sqrt{-1}) \tag{27a–c}$$

It can be seen that there are totally 24 unknowns ($n = 24$) in the $\boldsymbol{\beta}$ matrix and the number of unknowns is equal to the number of the degrees of freedoms of the element. It should be pointed out that n could be set to other numbers greater than $3m - 3$ ($3m$ is the total number of degrees of freedom of the element), however, it is recommended that the number of unknowns be equal to the number of the degrees of freedoms of the special element. Experience shows that a four-node special element with $N = 2$ could yield similar accurate results for the infinite plate problems considered later. Since the accuracy of the special element depends largely on how accurate of the displacements and electric potential on the special element boundaries, either more nodes (need more terms in Eq. (12)) or finer meshes (achieved by more special elements) are required for the special element to be used with other elements.

Substituting Eq. (12a–c) into Eq. (15a–e) yields the matrix $\mathbf{S}$ appeared in Eq. (16a) and matrix $\mathbf{U}$ in Eq. (16b). The traction vector $\mathbf{t}$ in Eq. (15c) can then be computed by using Eqs. (17) and (18). Since $\tilde{\mathbf{u}}$ is assumed along the element outer boundary only, interpolation along the element sides could be linear or quadratic depending on the type of displacement shape functions of the adjacent elements (Lee and Gao, 1995). The shape functions are to be chosen in parabolic forms in the following derivations. For example, along element side 1–3, matrix $\mathbf{L}$ in Eq. (19) is defined as

$$\mathbf{L} = \begin{bmatrix} N_1 & 0 & 0 & N_2 & 0 & 0 & N_3 & 0 & 0 & \underbrace{0\ldots0}_{15} \\ 0 & N_1 & 0 & 0 & N_2 & 0 & 0 & N_3 & 0 & 0\ldots0 \\ 0 & 0 & N_1 & 0 & 0 & N_2 & 0 & 0 & N_3 & 0\ldots0 \end{bmatrix} \tag{28a}$$

Along element side 3–5, matrix L in Eq. (19) is defined as

$$\mathbf{L} = \begin{bmatrix} \underbrace{0\ldots0}_{6} & N_1 & 0 & 0 & N_2 & 0 & 0 & N_3 & 0 & 0 & \underbrace{0\ldots0}_{9} \\ 0\ldots0 & 0 & N_1 & 0 & 0 & N_2 & 0 & 0 & N_3 & 0 & 0\ldots0 \\ 0\ldots0 & 0 & 0 & N_1 & 0 & 0 & N_2 & 0 & 0 & N_3 & 0\ldots0 \end{bmatrix} \tag{28b}$$

Along element side 5–7, matrix $\mathbf{L}$ in Eq. (19) is defined as

$$\mathbf{L} = \begin{bmatrix} \underbrace{0\ldots0}_{12} & N_1 & 0 & 0 & N_2 & 0 & 0 & N_3 & 0 & 0 & \underbrace{0\ldots0}_{3} \\ 0\ldots0 & 0 & N_1 & 0 & 0 & N_2 & 0 & 0 & N_3 & 0 & 0\ldots0 \\ 0\ldots0 & 0 & 0 & N_1 & 0 & 0 & N_2 & 0 & 0 & N_3 & 0\ldots0 \end{bmatrix} \tag{28c}$$

Along element side 7–1, matrix L in Eq. (19) is defined as

$$\mathbf{L} = \begin{bmatrix} N_3 & 0 & 0 & \underbrace{0\ldots0}_{15} & N_1 & 0 & 0 & N_2 & 0 & 0 \\ 0 & N_3 & 0 & 0\ldots0 & 0 & N_1 & 0 & 0 & N_2 & 0 \\ 0 & 0 & N_3 & 0\ldots0 & 0 & 0 & N_1 & 0 & 0 & N_2 \end{bmatrix} \tag{28d}$$

where

$$\begin{aligned} N_1 &= (s-1)(2s-1) \\ N_2 &= 4s(1-s) \quad s \in [0,1] \\ N_3 &= s(2s-1) \end{aligned} \tag{29}$$

where $s = S/L_{ij}$, S is the arc variable along the element side, and L_{ij} is the length of the element side ij.

To obtain the roots μ_k, Eq. (3) is rewritten as

$$\mu^6 + [(a_{11}\delta_{22} + 2a_{12}\delta_{11} + a_{33}\delta_{11} + b_{21}^2 + b_{13}^2 + 2b_{21}b_{13})/(a_{11}\delta_{11})]\mu^4 + [(a_{22}\delta_{11} + 2a_{12}\delta_{22} + a_{33}\delta_{22} + 2b_{21}b_{22} + 2b_{22}b_{13})/(a_{11}\delta_{11})]\mu^2 + (a_{22}\delta_{22} + b_{22}^2)/(a_{11}\delta_{11}) = 0 \tag{30}$$

or

$$\mu^6 + c_1\mu^4 + c_2\mu^2 + c_3 = 0 \tag{31}$$

Then μ_k can be conveniently obtained by solving the eigenvalues of the following matrix $\mathbf{P}$.

$$\mathbf{P} = \begin{bmatrix} 0 & -c_1 & 0 & -c_2 & 0 & -c_3 \\ 1 & 0 & 0 & 0 & 0 & 0 \\ 0 & 1 & 0 & 0 & 0 & 0 \\ 0 & 0 & 1 & 0 & 0 & 0 \\ 0 & 0 & 0 & 1 & 0 & 0 \\ 0 & 0 & 0 & 0 & 1 & 0 \end{bmatrix} \tag{32}$$

Thus, the stiffness matrix for the special element can be obtained by using Eq. (25).

5. Numerical examples

A computer program is written and several examples with known solutions are studied to test the proposed element. Gaussian quadrature is adopted to conduct the boundary integrations. The minimum number of Gaussian quadrature points is three. The material is assumed a PZT-4 ceramic. Reduced material constants provided by Sosa (1991) are

$$\begin{aligned} &a_{11} = 8.205 \times 10^{-12}\ \mathrm{m^2/N}; \quad a_{12} = -3.144 \times 10^{-12}\ \mathrm{m^2/N}; \\ &a_{22} = 7.495 \times 10^{-12}\ \mathrm{m^2/N}; \quad a_{33} = 19.3 \times 10^{-12}\ \mathrm{m^2/N}; \\ &b_{21} = -16.12 \times 10^{-3}\ \mathrm{m^2/C}; \quad \mathrm{b}_{22} = 23.96 \times 10^{-3}\ \mathrm{m^2/C}; \quad b_{13} = 39.4 \times 10^{-3}\ \mathrm{m^2/C}; \\ &\delta_{11} = 7.66 \times 10^{7}\ \mathrm{V^2/N}; \quad \delta_{22} = 9.82 \times 10^{7}\ \mathrm{V^2/N} \end{aligned} \tag{33}$$

It should be pointed out that one should be very careful in programming, since the order of material constants above are quite different which may result numerical instability or inaccuracy. The difficulty can easily be overcome, however, by adopting the modified units in the analysis (Sze et al., 2001). Attention should also be paid the plus–minus sign ± in Eq. (6) during numerical calculations. To ensure the accuracy, analytical data of Sosa (1991) in Figs. 3–9 have been recalculated.

Example 1. Consider the elliptical cavity shown in Fig. 2 with boundary conditions given by Eq. (34), namely,

$$\sigma_{ij}n_j = 0, \quad D_i n_i = 0 \quad (i, j = 1, 2) \tag{34}$$

For comparisons, far field mechanical loading in the x direction, different from the one shown in Fig. 2, is considered, namely, $\sigma_{xx}^{\infty} = \sigma_0$. And the maximum stress at $y = b$ is to be determined by the special finite element developed herein.

In the finite analysis, one special element proposed is used. For the infinite piezoelectric medium, set $H = W = 50$ mm, $a/H = 0.02$ if $a \geqslant b$ or $b/H = 0.02$ if $a \leqslant b$. The numerical results are listed in Table 1 for several a/b ratios. The results in Table 1 under the title "Elastic" is obtained by neglecting the terms containing the electrical variable. In other words, a purely anisotropic problem is solved. The data by the

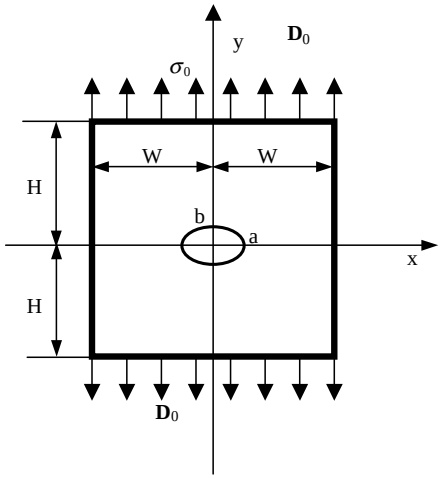

Fig. 2. Elliptical hole in an infinite or finite piezoelectric medium.

Table 1
Values of σ_{xx}/σ_0 at $x = 0$, $y = b$

a/b	Elastic			Electroelastic		
	Theory (Sosa, 1991)	Present (FEM)	% Difference	Theory (Sosa, 1991)	Present	% Difference
3	1.6222	1.623	0.06	1.743	1.742	−0.06
1	2.870	2.870	0.00	3.230	3.229	−0.03
1/3	6.610	6.610	0.00	7.700	7.682	−0.23
1/10	19.7	19.70	0.00	23.26	23.27	+0.03

finite element method are obtained by using the eight-node special hybrid stress element proposed by Zhan et al. (2003), a special case of the current element by taking out all electrical quantities. It can be seen that numerical results are compared very well with the analytical solutions for both "Elastic" and "Electro-elastic" cases. The efficiency of the proposed special element is demonstrated. It can be seen again by comparing the data listed in Table 1 that the differences between two theories are by no means negligible, pointed out earlier by Sosa (1991), thus the Electro-elastic theory should be used.

Example 2. Consider next an infinite piezoelectric medium with a circular hole (radius of a) under two different loadings, namely, either $\sigma_2^\infty = \sigma_0$ or $D_2^\infty = D_0$. The boundary conditions around the circular hole ($r = a$) are $\sigma_r = \tau_{r\theta} = D_r = 0$ if polar coordinates are used.

The finite element results for the stress σ_θ, electric displacement D_θ, electric field E_r and E_θ normalized with respect to the far field applied stress $\sigma_2^\infty = \sigma_0$ are shown in Figs. 3–5 (symbols), respectively. In the calculations, $H = W = 50$ mm, $a/H = 0.02$, to simulate the infinite piezoelectric medium. Only one eight-node special hybrid finite element is used in the analysis. To obtain the same accurate results for this problem, Deng and Wang (2002) used 1120 eight-node ordinary isoparametric elements to model a quarter of the plate. All numerical results are well compared with the analytical solutions (solid lines) given by Sosa (1991). The maximum values of σ_θ occur at $\theta = 0°$, 180°, and the maximum values of D_θ occur at $\theta = 65°$, 115°, agrees well with Sosa's theoretical results $\theta = 65°$, 114°.

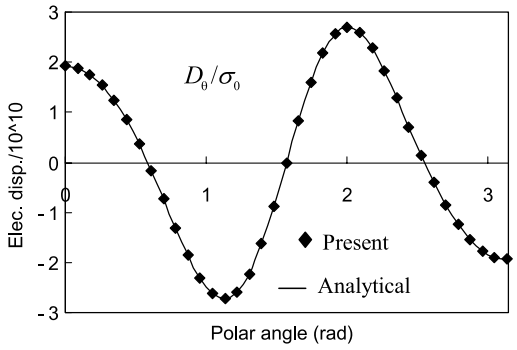

Fig. 3. Variation of D_θ with θ on the circular boundary under remote mechanical loading.

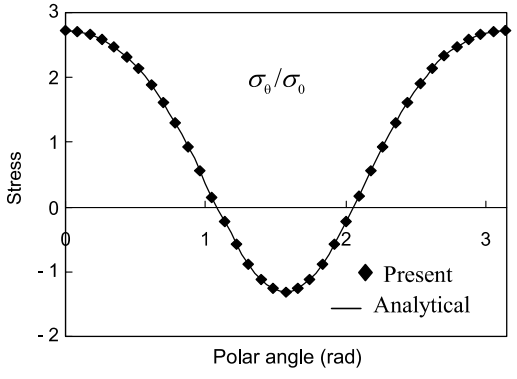

Fig. 4. Variation of σ_θ with θ on the circular boundary under remote mechanical loading.

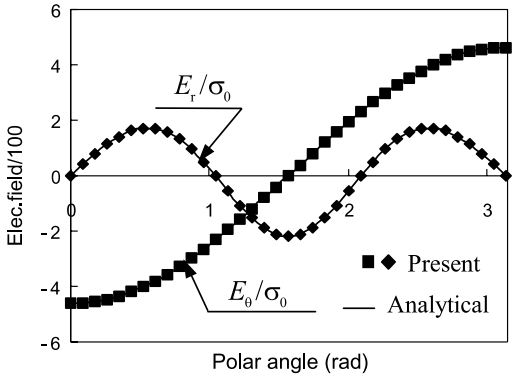

Fig. 5. Variations of E_r and E_θ with θ on the circular boundary under remote mechanical loading.

The finite element results for the stress σ_θ, electric displacement D_θ, electric field E_r and E_θ normalized with respect to the far field applied electric displacement $D_2^\infty = D_0$ are shown in Figs. 6–8 (symbols), respectively. Again the numerical data are well agreed with the analytical results (solid lines) of Sosa (1991) and Deng and Wang (2002). To achieve the same accuracy, 960 eight-node ordinary parametric elements

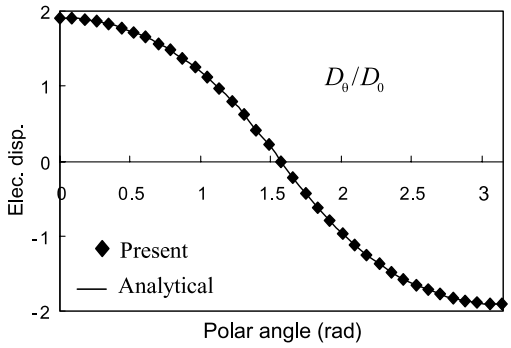

Fig. 6. Variation of D_θ with θ on the circular boundary under remote electrical loading.

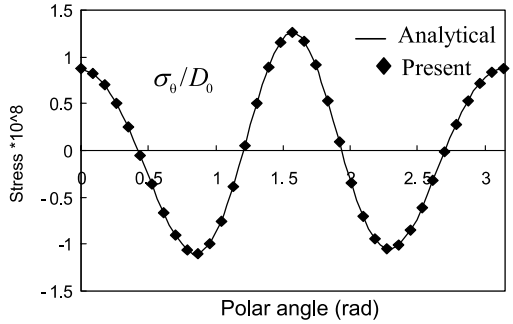

Fig. 7. Variation of σ_θ with θ on the circular boundary under remote electrical loading.

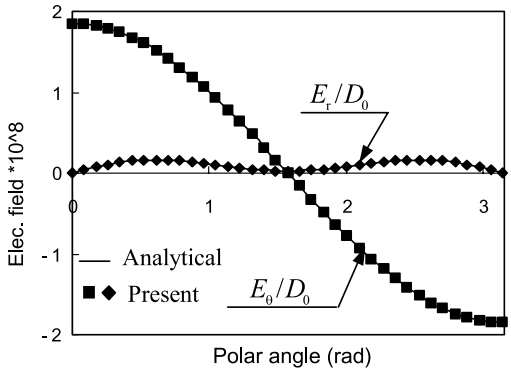

Fig. 8. Variations of E_r and E_θ with θ on the circular boundary under remote electrical loading.

are needed to model a quarter of the plates (Deng and Wang, 2002). It is obvious that the computational efficiency is high for the proposed finite element for this case.

Example 3. Consider the case of finite plates with a central hole under remote mechanical loading, $\sigma_2^\infty = \sigma_0 = 1$ MPa. Set $a = 1$ mm and vary W. The material is PZT-4 and the parameters are listed in Table 2 (Sze et al., 2001). The results obtained by using one special element are shown in Table 3 with various

Table 2
Material parameters of PZT-4 (Sze et al., 2001)

c_{11} (GPa)	c_{22} (GPa)	c_{33} (GPa)	c_{44} (GPa)	c_{55} (GPa)	c_{66} (Gpa)	c_{12} (GPa)	c_{13} (GPa)	c_{23} (GPa)
139	139	113	25.6	25.6	30.6	77.8	74.3	74.3
e_{15} $\left(\frac{C}{m^2}\right)$	e_{24} $\left(\frac{C}{m^2}\right)$	e_{31} $\left(\frac{C}{m^2}\right)$	e_{32} $\left(\frac{C}{m^2}\right)$	e_{33} $\left(\frac{pC}{vm}\right)$	ε_{11} $\left(\frac{pC}{vm}\right)$	ε_{22} $\left(\frac{pC}{vm}\right)$	ε_{33} $\left(\frac{pC}{vm}\right)$	
13.44	13.44	−6.98	−6.98	13.84	6000	6000	5470	

Table 3
Comparisons of the present data with results of conventional finite elements

W/a	Method (element no.)	$\sigma(a,0)/\sigma_0$	Relative error (%)	$u(w,0)$	Relative error (%)
	ANSYS (1280)	2.7464	2.68	-1.8234×10^{-10}	0.406
60	Present (1)	2.6728		-1.8308×10^{-10}	
	Analytical	2.6712			
20	ANSYS (1056)	2.7631	2.77	-6.2070×10^{-11}	0.161
	Present (1)	2.6865		-6.2170×10^{-11}	
16	ANSYS (1120)	2.7883	3.34	-5.0331×10^{-11}	0.227
	Present (1)	2.6952		-5.0445×10^{-11}	
12	ANSYS (1024)	2.7962	2.93	-3.8843×10^{-11}	0.402
	Present (1)	2.7142		-3.8999×10^{-11}	
8	ANSYS (1140)	2.8533	2.94	-2.8092×10^{-11}	0.783
	Present (1)	2.7694		-2.8312×10^{-11}	
4	ANSYS (1088)	3.1664	2.22	-2.1785×10^{-11}	0.179
	Present (1)	3.0959		-2.1746×10^{-11}	

W/a ratios. The computed normalized stress is at $x = a$, $y = 0$, and the displacement u at $x = W$, $y = 0$. The results by commercial software (ANSYS 7.1, element type: Plane 13) are also listed in the table for comparisons. It could be interesting to mention that ANSYS element Plane 13 is for coupled field analysis. The errors are absolute values by considering the ANSYS' data as the reference. The element numbers are 1 for the special element and vary slightly for the conventional elements. Fig. 9 shows a typical mesh for a quarter plate. From Table 3, it can be seen that the difference for the displacements are smaller than that for the stress. It is also found that the values of stress at $x = a$, $y = 0$ is relatively sensitive to the meshes generated by the ANSYS. Fig. 10 shows the stress distributions along $y = 0$ for the case of $W/a = 4$. It can be seen that the data obtained by the proposed special element agree well with the FEM results by ANSYS except at the $x = a$, $y = 0$. Thus, one may conclude that the proposed special element also works well for finite plates.

Example 4. Consider an infinite piezoelectric medium with a center crack of length $2a$ ($b = 0$) under combined mechanical and electrical loadings, namely, $\sigma_2^\infty = \sigma_0$ and $D_2^\infty = D_0$. D–P boundary condition is adopted around the crack surface.

To present the results and compare with analytical solutions, the polar coordinate system with the origin at the crack tip is introduced. Define $k = D_2^\infty/\sigma_2^\infty$ and $\sigma = \frac{\sigma_\theta\sqrt{2r}}{\sigma_2^\infty\sqrt{a}}$, where σ_θ is the stress computed at $r = 8\times10^{-4}$ mm in θ direction. The finite element results for stress σ are shown in Fig. 11 (symbols) with four different values of k (5×10^{-8}, 10^{-8}, -10^{-8}, 5×10^{-8}). In the calculations, $H = W = 60$ mm, $a/H = 0.02$, to simulate the infinite piezoelectric medium. Only one eight-node special hybrid finite element is used in the analysis. It can be seen that all numerical results are well compared with the analytical solutions (solid lines) of Sosa (1992).

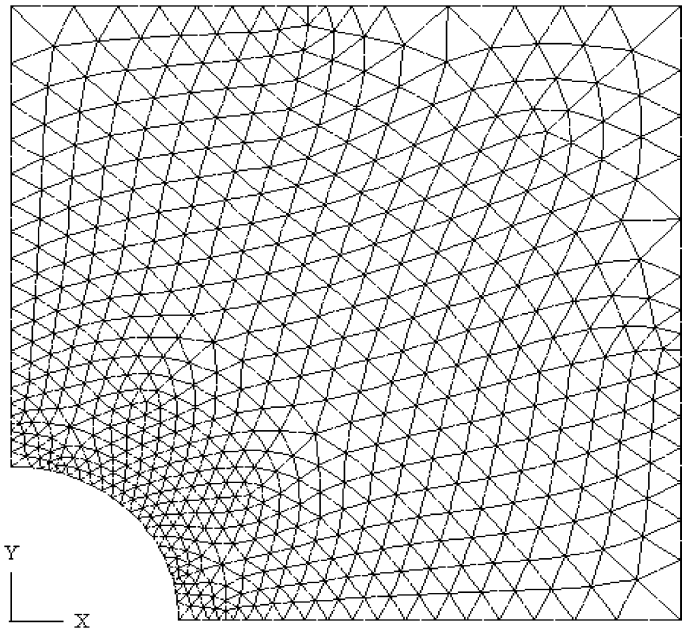

Fig. 9. Finite element meshes (ANSYS).

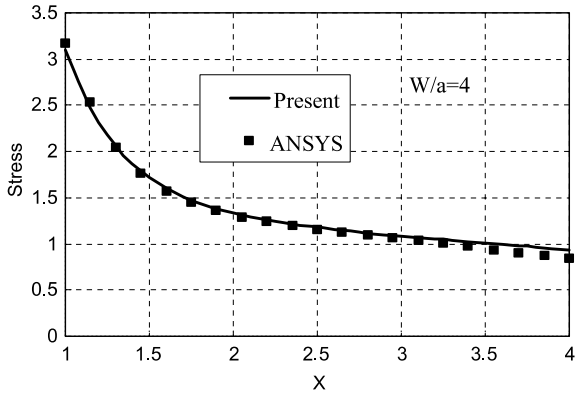

Fig. 10. Comparisons of stress distributions for a finite plate under remote mechanical loading.

Example 5. To investigate the performance of the special element to be used with other conventional elements or special element itself, a finite element mesh (11×11) shown in Fig. 12 is used to obtain the solution of the problem in Example 2. There are total 121 elements. Three cases are considered: Case 1. All are the same size special elements; Case 2. All are the eight-node conventional hybrid elements except the center one (special element) with same dimensions; Case 3. Top three rows (total 33 elements) and bottom three rows (total 33 elements) are eight-node conventional isoparametric elements and others are special elements with same dimensions. The normalize stress distributions in θ direction are shown in Fig. 13. As compared with the Sosa's analytical results, it is found that reduced the size of the special element (Case 1)

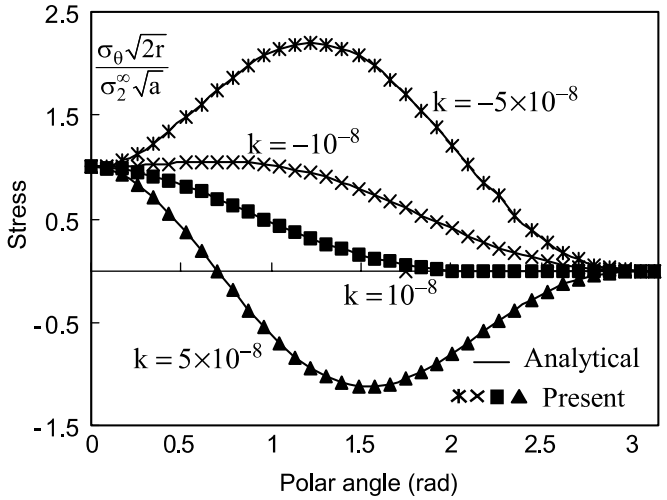

Fig. 11. Stress distributions around the crack tip under combined loadings ($k = D_2^\infty/\sigma_2^\infty$).

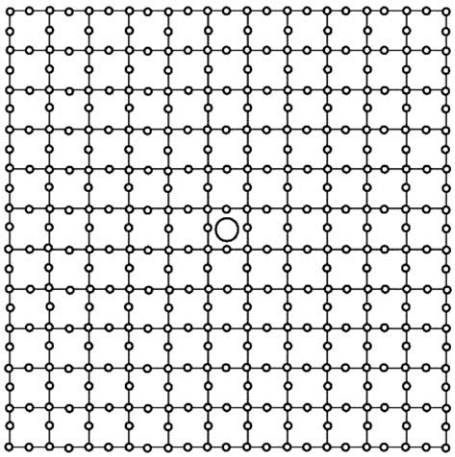

Fig. 12. Sketch of the finite element mesh.

does not degrade the performance of the element. In other words, finer meshes can be achieved by using more special elements if it is necessary. It is also seen that the performance of the special element with hybrid elements (Case 2) and the combination of special elements with conventional elements (Case 3) can also yield similar accurate results with finer meshes. It should be pointed out that the proposed special element works well with larger W/a ratios, while the conventional elements work well with smaller size. When the crack is not small compared with the rest of the structure, more nodes are needed for the special element to be connected with the conventional elements if it is required. This could be achieved either by introducing more terms in the series expression or by using more special elements (Case 1) then eliminate the inner nodes to compose a more nodes super element.

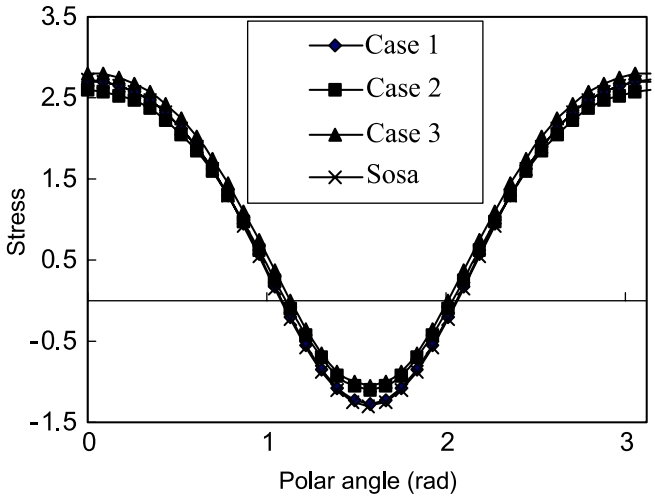

Fig. 13. Comparisons of σ_θ obtained by nine-element model with analytical data.

Example 6. Consider finite plates with a central hole under combined mechanical and electrical loadings. Outside dimensions of the plate are the same as considered in Example 3 and $W/a = 4$, while b/a varies from 1 to 0.0001. The reduced material constants in Eq. (33) are used in the analyses. Define $k = D_2^\infty/\sigma_2^\infty$, $K_s = \sigma_\theta/\sigma_2^\infty$, $K_d = D_\theta \times 10^{10}/\sigma_2^\infty$, and $K_{et} = E_\theta \times 10^2/\sigma_2^\infty$, the loading ratios, the concentration factors of tangential stress σ_θ, electrical displacement D_θ, and electric field E_θ at $x = a$, $y = 0$, respectively. The double logarithm plots, Figs. 14–16, show the variations of these three factors with b/a ratios, where series 1–3 correspond to the loading factor k taking the values of 0, 2×10^{-8}, -2×10^{-8}. It is interesting to see that the variations are fairly linear except for the stress concentration factor when loading $k < 0$. The sign of the electrical loading does not affect the linear relationships for the two electrical quantities, but does affects the linear relationships for the stress concentration factor a lot. The reason may be found in Figs. 17 and 18. Figs. 17 and 18 show the variation of K_s and K_d along the hole boundary when $b/a = 0.5$, where series 1–5 correspond to the loading factor k taking the values of 4×10^{-8}, 2×10^{-8}, 0, -2×10^{-8}, -4×10^{-8}. It can be seen from Fig. 17 that the maximum values of K_s are no longer at $x = a$, $y = 0$ but occurred at other places when $k < 0$, and K_s at $x = a$, $y = 0$ may be negative even for a tensile mechanical loadings. Thus, damage

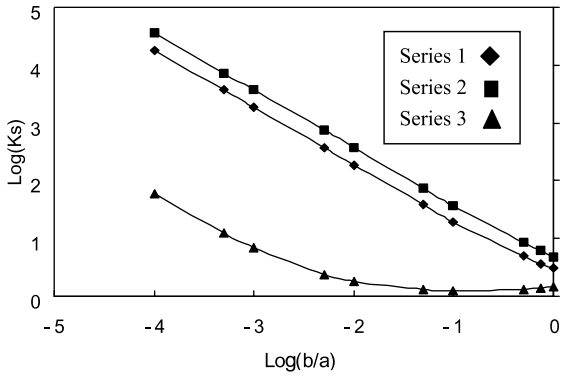

Fig. 14. Double logarithm plot of stress with hole size under combined loadings.

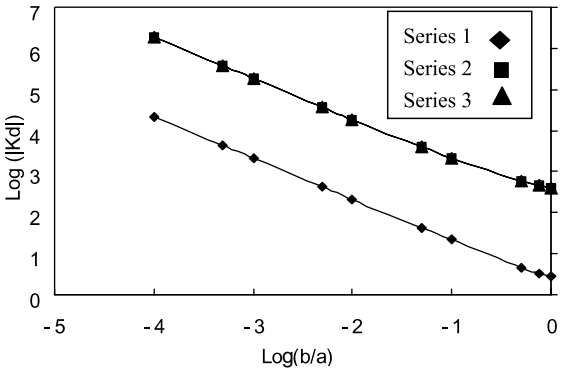

Fig. 15. Double logarithm plot of electric displacement with hole size under combined loadings.

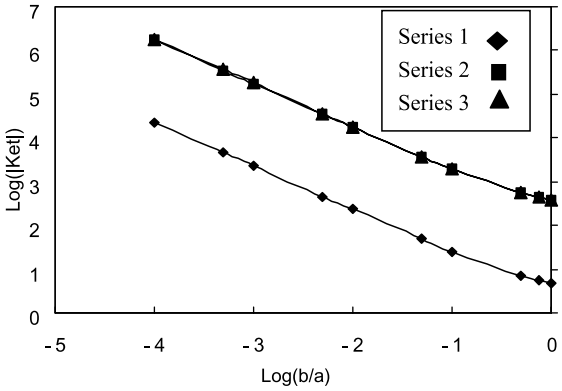

Fig. 16. Double logarithm plot of electric field with hole size under combined loadings.

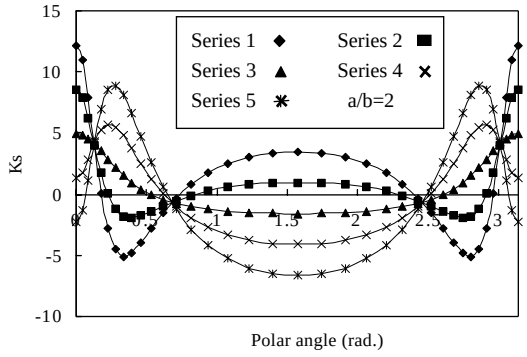

Fig. 17. Stress distribution around the hole under combined loadings.

may occur at places along the hole boundary otherthan at $x = a$, $y = 0$ under combined mechanical and electrical loadings. This may be the reason why the linear relationship does not hold in Fig. 14. It can be also seen from Fig. 18 that the sign of the loading factor does not alter the distribution of the electric quantities along the hole boundary if absolute values are considered. Thus, the linear relationship on the double logarithm plot (Figs. 15 and 16) holds for the electric quantities.

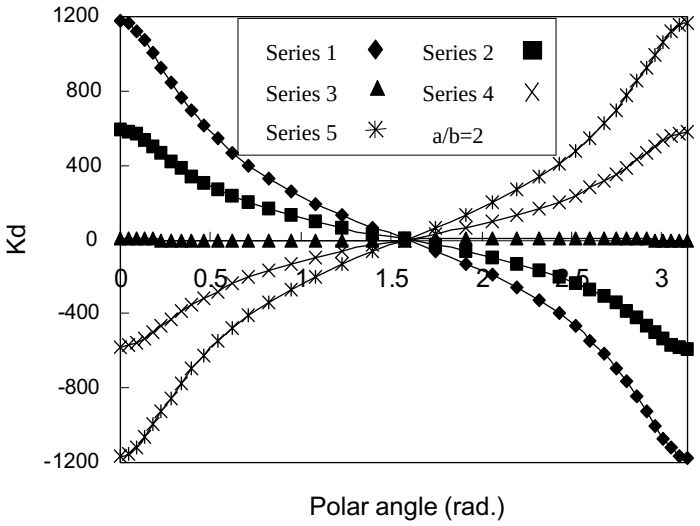

Fig. 18. Electric displacement distribution around the hole under combined loadings.

6. Conclusions

Special element containing an elliptical hole is developed for stress and electric field analysis of piezoelectric plates with defects. Numerical examples are performed to demonstrate the efficiency and accuracy of the developed element. It is observed that accurate results could be obtained around the hole in infinite and finite piezoelectric plates. For finite plates containing an elliptical hole under combined mechanical and electrical loadings, it is found that the relationship between the logarithm concentration factor of tangential stress, electrical displacement, and electrical field at $x = a$, $y = 0$ and logarithm b/a ratios is fairly linear for combined loads with positive electrical loading. Based on the results reported herein, one may conclude that the special element developed herein could be used as a super-element to reduce the finite element modeling effort in the analysis of the behavior of piezoelectric mediums with defects. It needs further investigation on the formulations and behaviors of the special element to deal with other electrical boundary conditions along the elliptical hole boundary or with inclusions.

Acknowledgements

The research is partially supported by National Natural Science Foundation of China (10072026, 50135030), China Ph.D. Foundation (20020287003). The reviewers' critical comments and information are sincerely appreciated.

References

Benjeddou, A., 2000. Advances in piezoelectric finite element modeling of adaptive structural elements: a survey. Comput. & Struct. 76, 347–363.

Chen, H.C. 1994. A special finite element with an elliptical hole for laminated structures, AIAA-94-1337-CP, pp. 253–263.

Chen, M.C., Sze, K.Y., Wang, H.T., 2001. Analysis of singular stresses in bonded bimaterial wedges by computed eigensolutions and hybrid element method. Commun. Numer. Methods Eng. 17, 495–507.

Chen, Z., Yu, S., 1999. Current research on the damage and fracture mechanics of piezoelectric materials. Adv. Mech. 29 (2), 187–196, in Chinese.
Chung, M.Y., Ting, T.C.T., 1996. Piezoelectric solid with an elliptic inclusion or hole. Int. J. Solids Struct. 33, 3343–3361.
Denda, M., Lua, J., 1999. Development of the boundary element method for 2D piezoelectricity. Compos. Part B 30, 699–707.
Deng, Q.L., Wang, Z.Q., 2002. Analysis of piezoelectric materials with an elliptical hole. Acta Mech. Sinica 34 (1), 109–114, in Chinese.
EerNisse, E.P., 1983. Variational method for electroelastic vibration analysis. IEEE Trans. J. Sonics & Ultroson. 14, 59–67.
Lee, J., Gao, H.J., 1995. A hybrid finite element analysis of interface cracks. Int. J. Numer. Methods Eng. 38, 2465–2482.
Lekhnitskii, S.G., 1981. Theory of Elasticity of an Anisotropic Body, English translation. Mir Publishers, Moscow.
Lu, P., Maharenholtz, O., 1994. A variational boundary element formulation for piezoelectricity. Mech. Res. Commun. 21, 605–611.
Lu, P., Williams, F.W., 1998. Green functions of piezoelectric material with an elliptic hole or inclusion. Int. J. Solids Struct. 35, 651–664.
Sosa, H., 1991. Plane problems in piezoelectric media with defects. Int. J. Solids Struct. 28 (4), 491–505.
Sosa, H., 1992. On the fracture mechanics of piezoelectric solids. Int. J. Solids Struct. 29 (21), 2613–2622.
Sze, K.Y., Wang, H.T., 2000. A simple finite element formulation for computing stress singularities at bimaterial interfaces. Finite Elem. Anal. & Des. 35, 97–118.
Sze, K.Y., Wang, H.T., Fan, H., 2001. A finite element approach for computing edge singularities in piezoelectric materials. Int. J. Solids Struct. 38, 9233–9252.
Tong, P., Pian, T.H.H., Lasry, S.J., 1977. A hybrid element approach to crack problems in plane elasticity. Int. J. Numer. Methods Eng. 11, 377–403.
Zhan, H.P., Wang, X., Zhou, H., 2003. An eight-node hybrid stress element with an elliptical hole for orthotropic materials. Acta Mech. Solida Sinica 24 (S. Issue), 128–132, in Chinese.
Zhao, J., Shan, H., 1991. Stress analysis around holes in orthotropic plates by the subregion mixed finite element method. Comput. & Struct. 41, 105–108.
Zienkiewicz, O.C., Taylor, R.L., 2000. The Finite Element Method, fifth ed. McGraw-Hill International Inc.